Journal of Material Cycles and Waste Management (2024) 26:1463–1479
https://doi.org/10.1007/s10163-024-01904-y

ORIGINAL ARTICLE

Thermal pre-treatment of reactive aluminium alloy waste powders

Roya Biabani[1] · **Piero Ferrari**[2] · **Mentore Vaccari**[3]

Received: 16 September 2023 / Accepted: 24 January 2024 / Published online: 11 March 2024

Abstract
This study focussed on assessing the efficiency of thermal pre-treatment of Al alloy waste powders to facilitate their subsequent treatment and disposal. Five samples originating from aluminium surface finishing industries underwent thermogravimetric analyses and were subjected to a laboratory tub furnace. Four set temperatures (450, 475, 500, 525 °C) for the tubular furnace were selected based on the TG results. Using sequential images of the sample inside the tubular furnace, the ignition delay time was calculated. In addition, the efficiencies of medium-temperature thermal pre-treatment were determined using the gas volume method. The shot blasting samples (S1 and S2) exhibited shorter ignition delay times compared to the sandblasting (S3) and one of the polishing samples (S4). The influence of ZnO alloy content on the ignition delay time was investigated, revealing that the ignition delay time decreased with an increase in ZnO alloy content. The raw and pre-treated materials were analysed for morphology, composition and reactivity. The pre-treatment efficiency of the samples improved, especially with a retention time longer than the ignition delay of the samples. Recommendations for the storage and handling of pre-treated products were provided.

Keywords Aluminium surface treatment · Hydrogen · Ignition · Reactivity · TG analysis · Tubular furnace

Introduction

Due to worldwide industrialisation and fast economic growth, industrial solid waste production has constantly increased over the decades. Amongst metals, aluminium as the second-most used metal globally has been used in a remarkably wide range of commercial goods in modern society due to its unique combination of characteristics such as softness, lightness, strength, excellent electrical and heat conductivity, low density and low melting point [1]. The most notable wastes generated in the aluminium production cycle are red mud, dross, grinding filter powder, furnace gas filter powder, skimming and salt cake [2]. Types of metallic wastes and their amounts vary depending on the raw materials used, operating conditions, the type of technology and furnace technology used [3]. Aluminium's natural tendency to corrosion leaves it looking dull through an aluminium oxide layer that forms over the metal to protect it. Towards increasing performance and service life of aluminium products, proper surface treatment technologies allow aluminium surfaces to remain pristine and prevent them from becoming tarnished or showing any signs of rusting. Metal surface technologies, such as brushing, polishing and sandblasting, generally imply phases that produce grinding filter powder, mainly as a by-product [2]. The expansions of aluminium dust during the processing, storage and transportation of bulk materials and powders have been characterised as an environmental hazard with the potential to cause harms to metal working area, waste transport and disposal systems [4]. Apart from the difficulties in managing the risk of dust explosions in metal working industries, the potential hazards of aluminium wastes disposal area have been studied by many researchers [5–9].

✉ Roya Biabani
r.biabanireshteh@studenti.unibs.it

Piero Ferrari
p.ferrari@brixiambiente.it

Mentore Vaccari
mentore.vaccari@unibs.it

[1] Department of Civil Engineering, Architecture, Land and Environment, University of Brescia, Via Branze 38, 25123 Brescia, Italy

[2] Research and Innovation at Brixiambiente Srl, 22 Via Molino Emili, Maclodio, Italy

[3] Department of Civil Engineering, Architecture, Land and Environment, University of Brescia, Via Branze 38, 25123 Brescia, Italy

At present, the traditional disposal methods (e.g. storing and landfilling) are greatly limited for the hazardous aluminium wastes. Aluminium waste dusts cannot be transferred to landfills because they will likely react amphoterically with water in the presence of hydroxyl ions and lead to inadvertent generation of hydrogen [10]. A study by Arm and Lindeberg [11] reported hydrogen explosions that occurred in landfills, rock caverns, old oil wells containing wet fly ashes caused by aluminium–water reactions. The overall reactions responsible for hydrogen generation in water–aluminium reaction are as follows [12]:

$$2Al + 6H_2O \rightarrow 2Al(OH)_3 + 3H_2 + Heat \quad (1)$$

$$2Al + 4H_2O \rightarrow 2AlO(OH) + 3H_2 + Heat \quad (2)$$

$$2Al + 3H_2O \rightarrow Al_2O_3 + 3H_2 + Heat \quad (3)$$

$$Hot\ H_2 + O_2(air) + combustibles \rightarrow fire \quad (4)$$

On exposure to oxidative atmospheres and temperature, an oxide film forms rapidly on aluminium particles surface, providing stability [13, 14]. According to Trunov et al. [15, 16], oxidation of pure aluminium, that is caused by a sequence of polymorphic phase transitions, occurring during the growth of the oxide film, can be divided into four main stages between 300 and 1500 °C. Whilst the thickness of the natural amorphous alumina layer increases slowly in the initial stage (300 °C < T < 550 °C), this layer transforms into γ-Al_2O_3 around 550 °C and this leads to a stepwise mass increase (the second stage). When pure Al reaches its melting point at ~ 660 °C, the transformation of γ-Al_2O_3 layer into θ-Al_2O_3 polymorph occurs (the third stage). Finally, as a result of the fourth stage, the α-Al_2O_3 is formed at temperatures above 1100 °C. Thus, the most probable aluminium–water reaction at room temperature is Eq. (1).

Shmelev et al. [17] and Rosenband and Gany [18] reported that the presence of a small fraction of activators enables a spontaneous reaction of activated aluminium particles even with cool water, which typically would not react with oxide or hydroxide surface layers. Nithiya et al. [19] confirmed the alkaline compounds in aluminium wastes. In a landfill, a highly exothermic reaction, which occurs when the water in contact with aluminium wastes become alkaline, between hydroxyl ions and aluminium metal inadvertently releases large amounts of flammable or toxic gases (e.g. hydrogen, acetylene, ammonia, carbon monoxide and benzene) [20]. Hydrogen gas from the amphoteric reaction of aluminium–water in the presence of hydroxyl ions is believed to be [20]:

$$Al_{(Metal)} + (OH)^{-1}_{(AQ)} + 3H_2O_{(Liquid)} \rightarrow \left[Al(OH^{-1})_4\right]^{-1}_{(AQ)} + 3/2H_{2(Gas)} + Heat \quad (5)$$

The consequences of the amphoteric reaction of aluminium within landfills are discussed by Stark et al. [20]. Their report showed that aluminium–water reaction may cause: (1) changes in leachate composition and quality; (2) undesirable increase in waste temperatures; (3) changes in gas composition and pressure with decreasing methane production and with increasing the generation of combustible and toxic gases; (4) microbial activity that would be considered desirable in anaerobic environments decreases; and consequently (5) the nuisance odours increase as a symptom surrounding the landfills.

Furthermore, fine particles of aluminium powder cannot be stored without specific safety precautions and considerations because they can readily disperse as a cloud in air due to their low masses. Upon dispersion in the air, which allows the particles to mix with oxygen, the burning occurs quickly so that an explosion results. Many studies have investigated the flammability of aluminium waste dusts produced by different metal industrial processes and the dust properties that contribute to explosions [21–27]. According to prevention and mitigation of dusts explosion with the concept of inherent safety, avoidance of dust cloud formation or control it below the minimum explosible concentration is fundamental [28]. Managing the risk of explosions in storages is not an easy task and lead to difficulties especially in small companies that often have limited resources.

Moreover, with increasing attention to the renewable high-calorie fuel such as hydrogen, there is a tendency to use aluminium and its alloys as the suitable metal source for hydrogen production. Therefore, disposal, utilisation and explosion control of this materials are receiving increasing attention in the future. According to the above concerns regarding the disposal of aluminium waste powders, it does not appear that any of the disposal methods alone would be effective in reducing the hazardous consequences that exist when aluminium explosible dust is present in quantities above its minimum explosive concentration. Therefore, reducing aluminium waste powders' reactivity as much as possible through thermal pre-treatment or thermal oxidation (not higher than 600 °C) may be the most promising approach, and then to determine the appropriate disposal (such as landfills) or utilisation (such as direction used in the formulation of porous concrete [29], fingerprint detection compounds [30], coatings and inks [31, 32]and hydrogen generation devices [33, 34] according to the risk assessment of residual reactivity level.

The utilisation of low–medium-temperature thermal treatment for waste disposal has increased due to its effectiveness and lower energy usage in recent years. Thus, in this study, the efficiency of medium-temperature pre-treatment of different aluminium waste powders from surface treatment industries, which applied a variety of processes to treat aluminium surfaces (e.g. shot blasting and polishing), was investigated. Implemented diagnostics including scanning and transmission electron microscopy (SEM), X-ray diffraction (XRD), sample weight monitoring in time and low heating rate reactivity analysis by thermogravimetry (TG) were utilised in this study. An analysis of thermogravimetric (TGA) data was performed to investigate the thermal behaviour of five different waste powders from aluminium surface treatment industries. Pre-treatment conditions were optimised by tubular furnace simulation experiments, and the total volume of the generated hydrogen before and after pre-treatment was examined.

Experiments

Materials and samples

The characteristics of the aluminium powders as by-products of metal working processes vary depending on the production techniques. A total of five aluminium waste samples were collected from different surface treatment industries. Surface treatment companies in Northern Italy use a variety of processes to treat aluminium surfaces, including shot blasting and polishing. In blasting, different blasting media are sprayed at high velocity onto the metal surface for the purpose of treating the metal surface. Blasting is mainly used to remove contaminants from the surface of castings, in preparation for subsequent finishing treatments, such as painting, enamel coating or mechanical treatment. Shot blasting is typically performed with rotating blade machines in which a stream of cleaning agents (steel grains or iron shots) is emitted, bombarding the casting's surface [35]. Instead, mechanical polishing process involves using abrasive media, flat wheels, sandpaper, wool berets, polishing sponges to remove scratches, nicks, and other surface defects created during the machining process. Polishing is a technique for improving the appearance and shine of the surface either manually or mechanically, thereby achieving the desired surface structure [36].

For this study, in three blasting factories that performed blasting on aluminium surface, dusts captured through drawholes and sent to a cyclone followed by a bag filter. Thus, three samples were collected from different grinding filter powders. In addition, two samples were collected from factories where polishing operations were conducted on aluminium products. According to the European Waste Catalogue adopted by Decisions (EU) N° 995/2014 and 1357/2014 of 18 December 2014 of the Council of the European Community, as amended by Decisions 2000/532/EC, all the samples found in this study are classified as hazardous waste according to the EWC 12 01 14* and 12 01 16* [37, 38]. Note that the purpose of this study is neither to assess the hazards associated with the samples nor to control their coding.

In this study, the effects of ZnO alloy powder as an additive on the ignition and oxidation properties of the samples were investigated. To prevent using raw materials, a zinc oxide alloy powder, which was produced as a waste in a metal industry, was utilised as an additive for decreasing the aluminium ignition delay time. The chemical composition of ZnO alloy powder is listed in Table 1. The mass fraction of the S3 and S5 to the ZnO alloy powder mixture was 1:1, 1:2 and 1:4 (w:w).

For decelerating the ageing of aluminium particles, fresh aluminium waste powders were rapidly stored in vacuum bags. The particle size distribution of the dust was realised on dry samples of about 50 g using a Ro-Tap Tyler mechanical sieve shaker equipped with Tyler mesh sieves. A balance with ± 0.0001 g sensitivity performed for weighing operations. The morphology of the samples was determined using a scanning electron microscope (SEM) with a Zeiss EVO MA10 (Carl Zeiss, Oberkochen, Germany). The X-ray diffraction (XRD) pattern was characterised on a D2 Advance powder X-ray diffractometer (Bruker, Karlsruhe, Germany). The elemental composition of the samples was determined through an acid digestion of 0.5 g waste with 15 ml of 37% hydrochloric acid and 5 ml of 65% nitric acid in a DigiBlock with 95 °C for 2 h. The cold digested samples were filtered on a Whatman grade 542 filters. Then metal contents determination was performed by means of an ICP Agilent Plasma Spectrometer.

Unreacted aluminium measurement

In this study, free aluminium content was indirectly determined by measuring the volume of gas released following the reaction between aluminium waste and NaOH solutions of 30 wt%. Due to strong alkalinity of NaOH solutions, aluminium–water reaction is quick [39]. As suggested by Zhu et al. [40] and Shi et al. [41], the efficiencies of the medium-temperature thermal pre-treatment of aluminium waste samples can be obtained by measuring the content of the unreacted Al in the sample after thermal pre-treatment. To determine unreacted aluminium in a sample, previous studies utilised volumetric techniques using hydroxide promoters such as NaOH, $Ca(OH)_2$, CaO and salt promoters such as NaCl [42]. Adding these components disrupts the

Table 1 Chemical analyses of the selected wastes produced in the aluminium surface treatment industries

Sample		S1	S2	S3	S4	S5	A
Waste European Code		12 01 16*	12 01 16*	12 01 16*	12 01 14*	12 01 14*	
Waste origin		Grinding filter powder; from shot blasting	Grinding filter powder with $CaCO_3$; from shot blasting	Grinding filter powder; from sand blasting	Grinding filter powder; from polishing	Grinding filter powder; from polishing	ZnO alloy powder
Organic matter	%wt	-	-	-	28.74	38.78	-
Mineral oil	%wt	-	-	-	8.29	5.14	-
Al	mg/kg	1,519,567.4	514,003.31	98,303.09	11,749.05	38,527.90	78,288.94
As		37.23	0.00	31.76	3.84	2.02	10.2
B		292.62	236.44	94.23	7.63	6.92	32.25
Be		0.03	0.04	1.11	0.03	0.06	0
Cd		1.10	0.00	59.91	0.97	0.28	3.31
Co		0.00	0.00	51.68	0.00	0.85	236.97
Cr		42.21	47.33	2747.14	24.89	21.59	512.18
Cu		1351.26	874.58	3635.68	781.03	1146.02	9647.06
Mg		5386.44	43,971.9	702.22	300.34	409.63	6058.45
Mn		147.04	182.94	5457.92	167.19	115.29	491.07
Mo		32.99	12.63	128.2	2.20	2.26	30.75
Na		1076.24	566.24	364.3	286.89	487.78	48,406.97
Ni		108.47	72.40	1244.07	9.26	32.27	2712.72
Pb		530.02	351.04	944.86	92.04	53.56	338.65
Sb		146.9	91.84	99.05	7.7	5.84	66.51
Se		11.85	5.26	0.00	0.27	0.22	52.06
Sn		19.35	15.80	41.30	1.82	6.23	16.6
Tl		214.35	246.1	86.97	6.42	9.93	1.59
V		0.00	0.00	0.00	0.00	0.00	431.32
Zn		345.22	294.55	71,895.44	52,958.52	620.08	138,160.47

Attention: 12 01 14* machining sludges containing dangerous substances

12 01 16* waste blasting material containing dangerous substances

aluminium oxide layer on aluminium particles and releases hydrogen gas.

The schematic of the hydrogen generation and alkaline water–aluminium reaction temperature systems used in the experiment is shown in Fig. 1 (a). Equation 6 shows the water–aluminium reaction in the presence of NaOH as a hydroxide promoter [43].

$$2NaOH + 2Al + 2H_2O \rightarrow 2NaAlO_2 + 3H_2. \quad (6)$$

Here are the equations that can be used to calculate the unreacted Al content in thermal pre-treated products [43][43]:

$$n_{H_2} = V/22400 \quad (7)$$

$$n_{Al} = n_{H_2}/1.5 \quad (8)$$

$$W_{Al}^{S} = 26.98\left(\frac{g}{mol}\right) \times n_{Al} \quad (9)$$

$$W_{Al}^{P} = W_{Al}^{S} \times W_P/W_S \quad (10)$$

$$\eta = (W_{Al} - W_{Al}^{P})/W_{Al} \times 100 \quad (11)$$

where V refers tothe volume of hydrogen produced by the reaction of unreacted aluminium with NaOH-water (ml); W_{Al}^{S} is the mass of aluminium in the tested sample (g); W_S, W_P and W_{Al} are the mass of tested sample (g), the total mass of the thermal pre-treated product (g) and the total mass of Al in the original sample, respectively; W_{Al}^{P} is the total mass of aluminium in the thermal pre-treated product. Moreover, η refers to the thermal pre-treatment efficiency.

TGA test

The determination of the parameters of non-isothermal oxidation under the standard conditions of programmed heating in an atmosphere of air can be utilised to compare the reactivity of the powders [45]. Parameters for an evaluation of

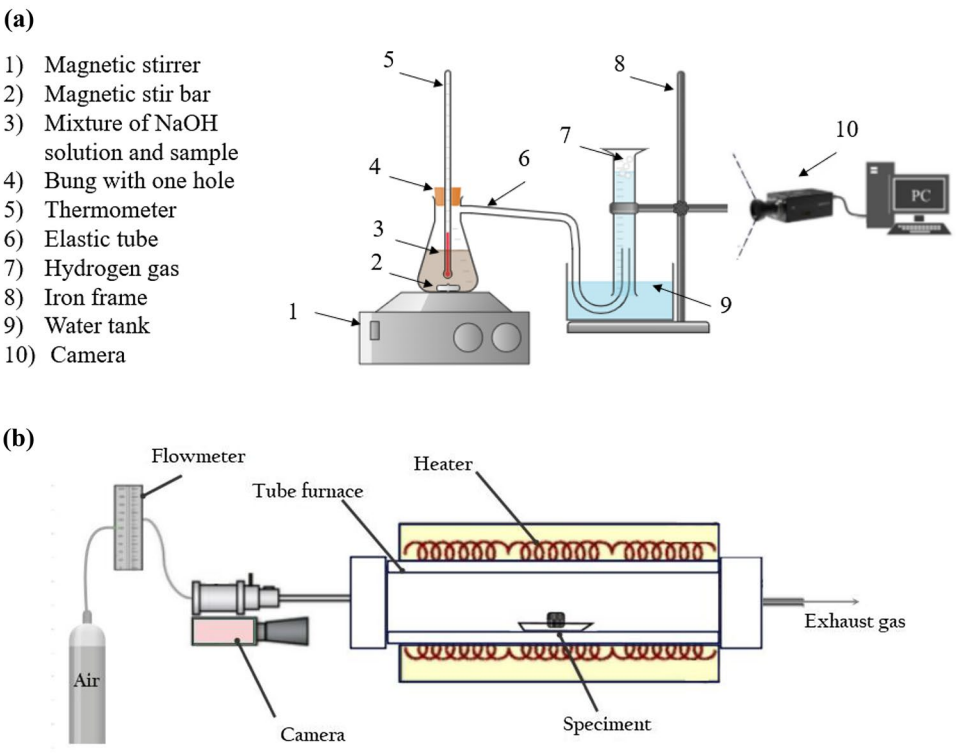

Fig. 1 Schematic diagram for the experimental systems; **a** gas volume measurement system; **b** tubular furnace

the reactivity of powders, including temperature of intensive oxidation onset (T_{on}, °C), the mass gain at the first oxidation step (α_I, mass %) and the total mass gain at the end of the oxidation process (α_T, mass %), can be obtained during the processing of the results of non-isothermal oxidation under standard conditions of programmed heating in an atmosphere of air using thermogravimetric analysis (TGA) and differential thermal analysis (DTA) curves [46, 47].

The medium-temperature thermal pre-treatment characteristics of aluminium powder wastes under nitrogen atmosphere (anaerobic condition) and air atmosphere (aerobic condition) were tested by heating the fine powder samples (~5 mg) in an open Pt crucible from room temperature to 1000 °C at the rate of 10 °C/min in a thermogravimetric Q5000 apparatus (TA Instruments, New Castle, DE, USA) interfaced with a TA5000 data station. Then to achieve 25 °C, the instrument was ventilated until it was completely cooled.

Tubular furnace simulation experiments

Four different furnace set points (450, 475, 500 and 525 °C) were selected based on the TGA to identify the ignition delay time, the optimum heating time and to evaluate the efficiency of medium-temperature thermal pre-treatment for reduction of the reactivity of aluminium waste samples. The tubular furnace consists of an air cylinder, a tube furnace and a temperature controller (Fig. 1 (b)). When the temperature of the tube furnace reached the set temperature, the air with the flow rate of 300 (l/h) was continuously fed into the quartz tube for 15 min to ensure that air was exhausted. Then an alumina boat (105×14×9 mm) was loaded with sample (~70 mg), and then it was placed into the centre of the tube furnace.

Ignition delay is the amount of time necessary to destroy the weak oxide film on the surface of Al particles that allows the fresh aluminium core to easily react with oxygen to form a strong oxide film in the presence of temperature. To obtain the ignition delay time of each sample, a video camera was used. In this experiment, ignition delay time (t_d) was interpreted as the duration of time between when sample appeared below window and the first combustion phenomenon occurred. The ignition delay time was captured utilising a video camera and the ignition delay time (t_d) is as follows:

$$t_d = t_i - t_0 \tag{12}$$

where t_0 is the time of the first image of the sample captured inside the tube furnace and t_i is the time corresponding to the first appearance of ignition phenomenon of sample.

Results and discussion

Basic characteristics of the samples

The main elements identified in each sample are listed in Table 1. The most abundant element in the analysed samples was Al. Amongst the elements discovered were Cu, Mg, Pb and Zn, as well as other elements at low concentrations. The identified elements included Cu, Mg, Pb, Zn and other elements at low concentrations (Table 1). The S4 and S5 were obtained from polishing processes. Therefore, these samples contained a certain amount of the mineral oil and organic matters depending on the age of the polishing tools, and on the pressure and speed adopted to polish the pieces. Although the amounts of these components were relatively low, they constituted a major effect on the particle size distribution and the reactivity behaviour of the samples.

According to the scanning electron microscope images of the samples (Fig. 2), it can be concluded that the morphology of the samples is affected to a great extent by the manufacturing process that generates the powders. The powders feature mainly non-spherical. In general, the particle texture appears cluster with smooth surface. In the case of shot blasting samples (Fig. 2(a), (b) and (c)), the repeated fragmentation of particles during blasting causes mechanical breakage of the oxide film and consequently provides the direct contact between oxidiser and fresh surfaces of aluminium. Moreover, some zinc oxide particles have been stuck to aluminium particles during blasting.

The particle size distribution for all tested samples is illustrated in Fig. 2(f). As shown, samples associated with blasting processes contain a high proportion of fine particles. For instance, about 94% particulate S1 compounds by

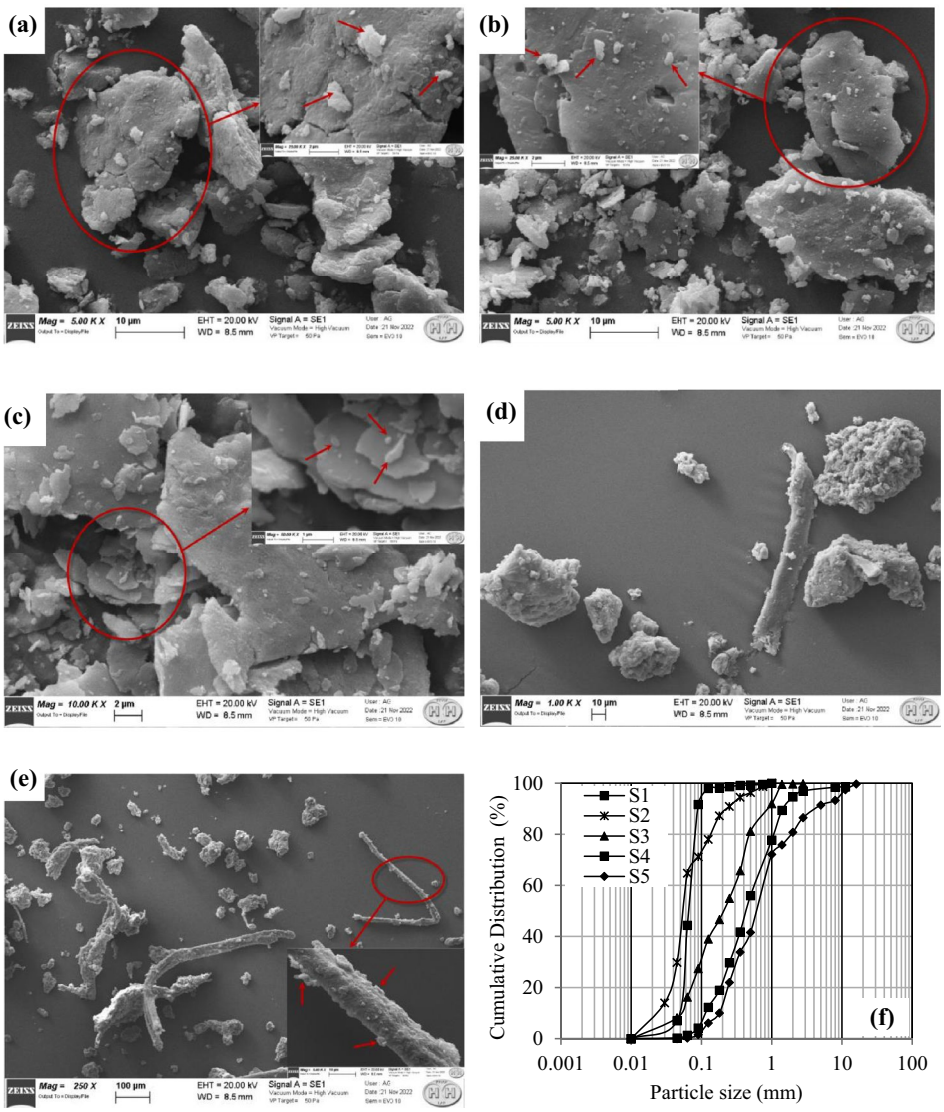

Fig. 2 SEM characterisation of the tested samples: **a** the S1; **b** the S2; **c** the S3; **d** the S4; **e** the S5; **f** particle size distribution of the tested samples

weight were less than 0.1 mm diameter and 66 wt% was less than 0.05 mm. The sample S5 has a fraction over 1 mm about equal to the 30 wt%. However, a total of 22 wt% of the S4 remained over the sieve 1 mm. Essentially, the residues left behind using cloth, brushes and sponges to polish the surfaces were remained in this range. The polisher material residues vary in quality and quantity depending on the technique used for polishing a metal surface. The organic matter test revealed 38.78 wt% of the S5 contains organic matters that consists mainly of long threads of organic residues of polishers (Fig. 2(d) and (e)). The organic content of the S4 was about 28.74 wt%.

The remained samples over each sieve were collected and tested to determine the effects of particle size on reactivity of the samples (Fig. 1 s). For the S1, results demonstrated that reactivity, which implies the content of metallic aluminium in powders, increases with decreasing particle size. This result is in agreement with the previous studies' conclusion that metal content of such powders typically decreases with increasing particle size [48, 49]. However, for the polishing samples, the remained samples over sieve 1 mm interestingly release more hydrogen gas with respect to the samples with particle size less than 125 µm. Testing for mineral oil revealed that the Samples 4 and 5 contained 8.29 wt% and 5.14 wt% mineral oil, respectively. Mineral oil was used in polishing processes basically because of its excellent lubricating properties. Generally, in polishing processes, mineral oil was absorbed by polisher materials. As a result, micro- and nano-sized aluminium waste particles were trapped by mineral oil, and they were attached to polisher residues. This might explain the reason of higher reactivity of larger particles compared to those with smaller particles in the S5. Due to the organic content, temperature increase and release of combustible gas associated with hydrolysis of aluminium, the polisher residues of the S4 and S5 require treatment.

Hydrogen generation capacity of the raw samples

Figure 3(a) shows a trend of changing hydrogen production (normalised with the weight of tested sample) with increasing reaction time. When the activator solution (NaOH) remains constant in all runs, the hydrogen production start time and the hydrogen production volume of each sample are unique and dependent on both granulometry and chemical properties of the samples. Although the S2 showed the fastest response to the alkaline water solution, 74.4% of the volume of hydrogen which measured after 24 h was released within the first hour of the reaction. Because of the greater proportion of the particles smaller than 0.5 mm, the S2 has the fastest start time whilst its aluminium content is lower

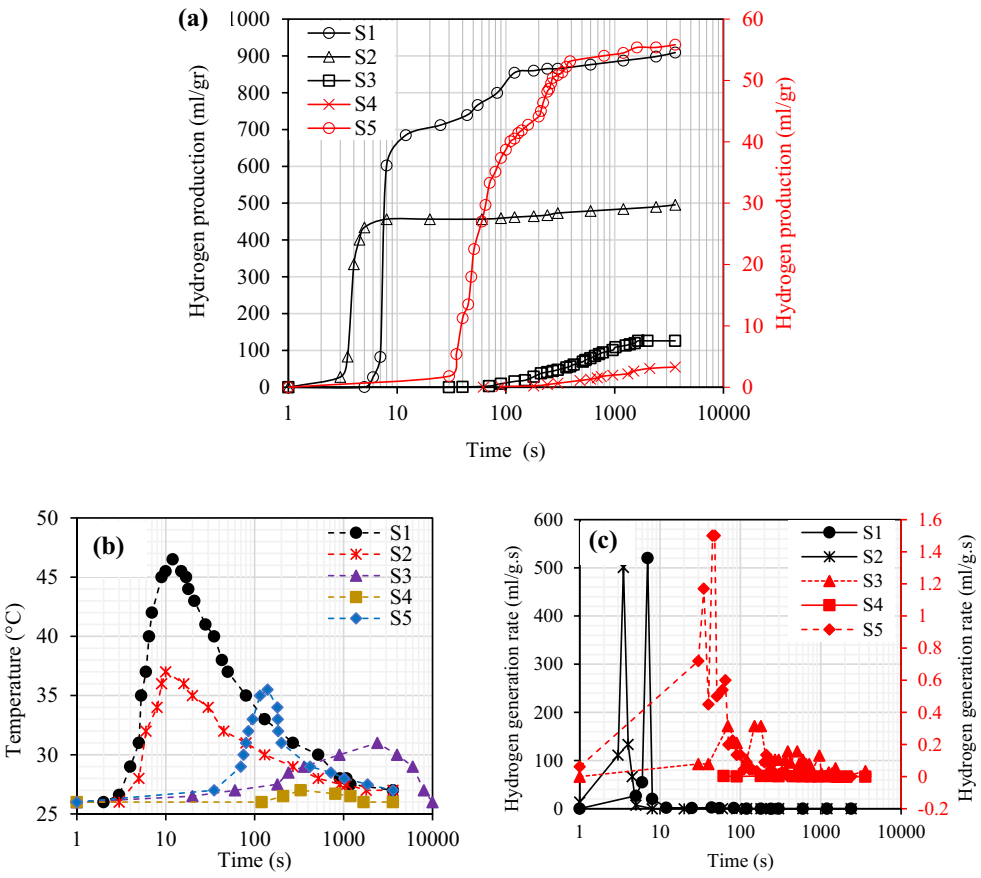

Fig. 3 **a** Hydrogen production of different samples over an hour; **b** temperature change during the reaction of aluminium and alkaline water; **c** hydrogen generation rate during the reaction of aluminium and alkaline water

than the S1. The S1 released 87.62% of its long-term measured hydrogen in the first hour of the reaction. For the S1 and S2, a large volume of gas was observed in a short period of time after starting the reaction, indicating their potential hazard in the presence of hydroxide promoters. Compared to other blasting samples, the corresponding hydrogen production start time of the S3 took longer than the other blasting samples because of its greater granulometry distribution. Following the first hour of the reaction, the hydrogen production equalled 69.16% of those corresponding to the long-term production.

A lower aluminium content in the polishing samples resulted in significantly small hydrogen production. Therefore, to identify the hydrogen generation changes during the reaction time, the corresponding values for the S4 and S5 were shown in the second Y-axis. Due to the more aluminium content of the S5 compared to the S4, spontaneous alkaline water–aluminium reaction of the S5 is faster. The results of the S4 and S5 revealed that 22.16% and 99.73%, respectively, of the long-term hydrogen production were achieved within the first hour of the reaction.

The effects of different aluminium waste samples on alkaline water temperature changes are illustrated in Fig. 3 (b). A significant temperature rise occurred for the S1. The alkaline water temperature increased from 26 to 46.5 °C in 12 (s) for the S1 whilst increasing to 37 °C was observed in 10 s for the S2. The alkaline water temperature changes for the S3, S4 and S5 were 5 °C, 1.5 °C and 11.5 °C, respectively. A similar finding corresponding to the rise of temperature in alkaline water–aluminium reactions was reported by Cai et al. [42] and Li et al. [50]. A comparison of Fig. 3(b) and (c) indicates that hydrogen generation rate is associated with alkaline water temperature rise. As shown, the temperature of alkaline water increases just before hydrogen is released due to the oxidation reaction. This confirms the Rosenband and Gany's [18] conclusion that an increase in alkaline water temperature likely further accelerates hydrogen production rate. Consequently, due to elevated temperatures and explosive gases produced by leachate hydroxyl ions shortly after aluminium samples are dissolved in water, the samples cannot be disposed in landfills without being pre-treated.

Thermal reaction characteristics of the tested samples

Figure 4 shows the TGA and DTG curves of the samples measured under anaerobic and aerobic conditions at a heating rate of 10 °C/min. Different samples exhibited significantly different TGA profiles. For the S1, it is possible to distinguish three main mass change steps. The first mass loss stage is from room temperature to about 400 °C with 2.3% mass loss which can be due to the solvent release. Then it follows with two continuous mass gain steps. The first mass gain step of about 9.7% ends at 720 °C. In the corresponding DTA curve, an exothermic peak is suddenly affected by the latent heat of aluminium melting at 600 °C. Then the second intense mass gain step (about 34.9%), which not yet concluded at 1000 °C, took places. This intense mass gain in the second step is because of the melting of Al which causes the volume expansion of Al core and resulting in compress pressure within the tensile stress on the oxide film and the Al core. Therefore, the samples S1 exhibit significant mass gain (around 37%) since the oxidation of Al between 400 and 1000 °C. Moreover, the slope of the mass gain steps indicates the oxidation rate of the sample which decreases with increasing the reaction time. Since the thickness of oxide film on the Al surface increases, the slope of mass gain branch or reaction rate decreases.

On the contrary, under nitrogen atmosphere, the S1 shows a slow mass loss from room temperature up to 500 °C, that mass loss step can be due to the solvent release. Although nitrogen is considered as a nearly inert gas, aluminium nitride forms when aluminium is heated above 830 °C in atmosphere of nitrogen and the reaction involve is Eq. 13 [51].

$$2Al + N_2 \rightarrow^{\Delta} 2AlN \tag{13}$$

The DTA curve (Fig. 4 (a)) can be used to investigate the reaction between nitrogen and aluminium. The DTA curve shows an exothermic peak around 820 °C probably related to the aforementioned reaction. As concluded by Saravanan et al. [52], aluminium and nitrogen react even at temperatures as low as 850 °C. Therefore, the consistent mass gain between 500 and 1000 °C is mainly due to the transformation of Al to AlN.

To reduce or eliminate the fire and explosion likelihoods, the manufacturer that produced the S2 added calcium carbonate powder as an inert powder into a bag filter powders. By means of thermogravimetric analysis (TGA), influences of $CaCO_3$ on oxidation process and thermal behaviours of aluminium waste powder are shown in Fig. 4 (b). Under air atmosphere, the TGA curve includes four weight change steps. With regard to the solvent release, there is a weight loss step during heating up the sample at 25–575 °C. By increasing the temperature up to 610 °C, there is a continuous weight gain in the TG curve resulting from oxidation process of Al particles. In the zone of 610–730 °C, the TGA/DTA curve is indicative of the overlapping of one peak of exothermic reaction and two peaks of endothermic reactions. The intensity of the endothermic process of the decomposition of $CaCO_3$ and the process of aluminium melt has overshadowed the exothermic process of oxidation. Because of this, the DTA curves cannot depict these stages clearly. By continuing to increase the temperature up to 1000 °C, a noticeable mass gain is achieved due to the oxidation

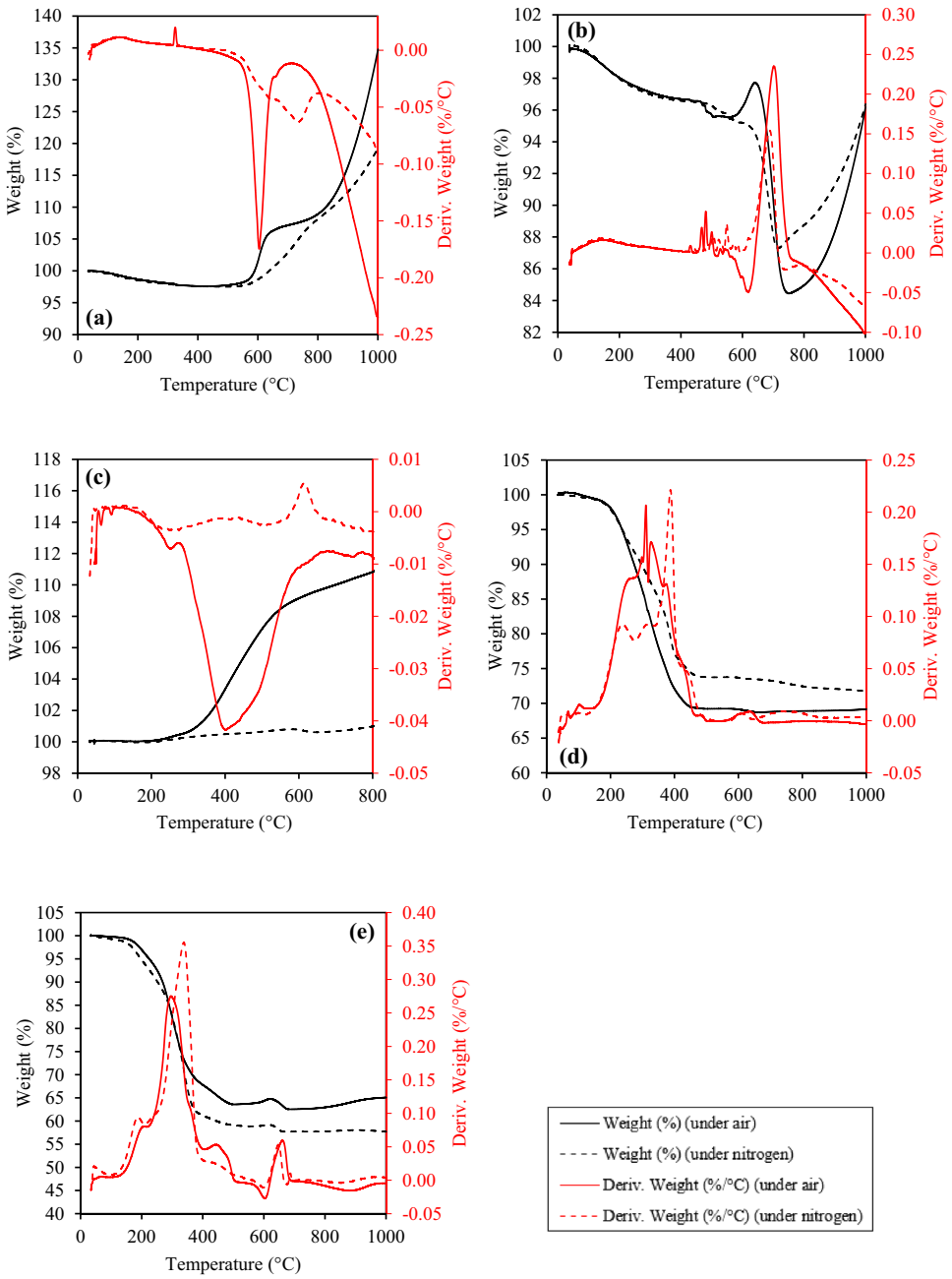

Fig. 4 TGA/DTA curves of **a** the S1; **b** the S2; **c** the S3; **d** the S4; **e** the S5

process, although the gain has not completed. Decomposition of calcium carbonate similarly affects the oxidation behaviour of the S2 under N_2 atmosphere (Fig. 4(b)). However, the total mass gain value obtained for N_2 atmosphere differ considerably from those obtained from air atmosphere.

The corresponding TGA curves of the S3 are shown in Fig. 4(c). In air atmosphere, there is no mass gain or any mass loss to the temperature limit of 200 °C. This is indicative of the fact that no significant oxidation or decomposition has taken place within the temperature range of room temperature to 200 °C. As the temperature is increasing, a continuous mass gain is started around 200 °C and the mass gain has not been completed at 1000 °C. The production process of the S3 may give insight into why oxidation is taking place at such low temperature (at 200 °C). During the production of the S3, the manufacturer applies solid lubricants to burnish and compact the coating, thereby optimising the surface area of the coating on the substrate. Solid lubricants can react and be oxidised with exposure to temperature. Along with this mass gain, an exothermic peak is not observed in the DTA curves between 200 and 1000 °C. Whilst the temperature increases, the oxidation of the metals takes place, leading to increase in the mass gain reaching a total of about 12.31% at 1000 °C.

Figure 4(d) shows the baseline-corrected TGA and DTA traces for the Samples S4 under air and nitrogen atmosphere, respectively. In nitrogen atmosphere, after a solvent release step (0.8% up to 125 °C), a first mass loss ending at around 275 °C leads to a 10% mass loss. After this, releasing the organic matters with low evaporation temperature takes place, ending at 320 °C (3.4%). Then it follows with an intense mass loss step at 350 °C (see the DTG peak) due to the desorption of organic matters with high evaporation temperature. By increasing the temperature, two further mass variations of 0.3% and 3% take place between 510 °C and 650 °C and from this temperature value to 1000 °C, respectively. The total mass loss of the S4 is about 31%. In addition, the S4 shows mass loss steps under air atmosphere. However, it is less distinguishable. A first multi-step process, from 125 to 525 °C, leads to a strong mass loss of 30.8%. This mass loss step mainly occurs because of the desorption of organic matters. Finally, a small mass increase of 0.4% is detected between 650 and 1000 °C, indicating that Al particles react with oxygen in the chamber.

For the sample S5, the solvent release ends at about 100 °C under nitrogen (Fig. 4(e)). A desorption step accounting for 6.2% mass gain takes place, ending at 205 °C. Subsequently, due to the presence of organic matters with the high evaporation temperature, a strong mass loss (34.8%) is recorded up to 600 °C, including 4 steps which the most important one was ended at 410 °C. The mass remains constant starting from 800 °C. However, the total mass loss is about 42.34%. Under air, Sample S5 shows a negligible solvent release (Fig. 4 (e)). By increasing the temperature, a 4-step decomposition process accounting for 36.4% mass loss is recorded from 100 to 500 °C. From 530 to 620 °C, a 1.2 wt% mass gain is recorded, and then a 2.2% mass loss ends at 700 °C. A further increase in temperature leads to a mass gain of about 2.5% at 1000 °C.

Pre-treatment simulation experiment of the samples in a tubular furnace

The blasting samples and polishing samples showed different combustion behaviour inside the furnace (Fig. 2s). When the blasting samples (S1 and S2) are loaded into the tube furnace, they absorbed heat and slowly turned red. Depending on the furnace set point, chemical composition of the samples, and more importantly the thickness of oxide shell which has been formed due to the ageing of Al particles, the S1 and S2 are ignited after a specific delay times. First, the samples are partially ignited, then the combustion area spreads out. The brightness of combustion area of the S1 is obviously higher than that of the S2, indicating that the release heat of the S1 is larger. As the S1 and S2 ignited, the tube furnace temperature increased, verifying the release of heat. Both samples exhibit the highest ignition delay at 450 °C and it decreases with increasing the furnace set point. In comparison with the S1, the S2 has a relatively low Al content, but it showed a strong ignition at the tested temperatures. This is principally because of its high percentage of small particles with large self-heating rate, which becomes dominant for the ignition of Al particles [15, 16]. In addition, a considerable percentage of magnesium (Mg) as an alloying component leads to decrease the Al ignition delay time and temperature [53].

The reduction efficiency of hydrogen production of Al powder represents its effectively oxidised amount, which is a very important parameter to characterise the reactive Al content. For estimating the effect of heating time on thermal treatment efficiency to reduce the reactivity of different samples, unreacted Al content was calculated by measuring the volume of gas (Sect. 2.2). According to Fig. 5 and Table 2, the samples that are taken out of the furnace before ignition occurs are much more reactive than those left inside the furnace for longer periods of time. This is because the ignition causes the weak alumina shell on the Al particle surface to be broken, and the exposed active Al rapidly reacts with oxygen. Therefore, ignition contributes to an important heat feedback mechanism for influencing the oxidation rate.

The XRD patterns of the combustion products of the tested samples, after being heated in the tube furnace, are shown in Fig. 3s, the diffraction peaks of metal oxide be detected. In the SEM images shown in Fig. 6, the combustion products of the S1 and S2 are submicron needles, and the combustion products of the S3, S4 and S4 are spheres. Thus, the microstructure of the combustion products of all the tested samples changed radically in comparison with the initial powders. Obviously, the appearance of combustion products in the form of needles of submicron diameters results from participation of the gaseous phase in the formation of the final products [54].

The S3 without an additive cannot be ignited at any of the tested furnace set points, so its ignition delay time is not presented in Table 2. Some methods have been introduced to improve the ignition of Al particles. One approach is to increase the proportion of nano-sized Al compared to micron-sized Al since nano-sized Al particles have lower ignition temperature and faster burning rate [55, 56]. In addition, for the enhancement of the ignition process of Al powders, Al can be blended with some materials. Many efforts have been made to understand the effects of different additives (e.g. chromium chloride ($CrCl_3$) [57], sodium fluoroaluminate (Na_3AlF_6) [41], sodium fluoride (NaF) [39], potassium fluoride (KF) [58], nickel (Ni) [59], magnesium (Mg) [60], silicon (Si) [61], silica (SiO_2) [62], zinc addition [63]) on pure aluminium/aluminium alloys' thermal characteristics. Since resources shortage and environmental concerns are increasing, moving towards a resource-efficient and circular economy is essential. Waste prevention target defined

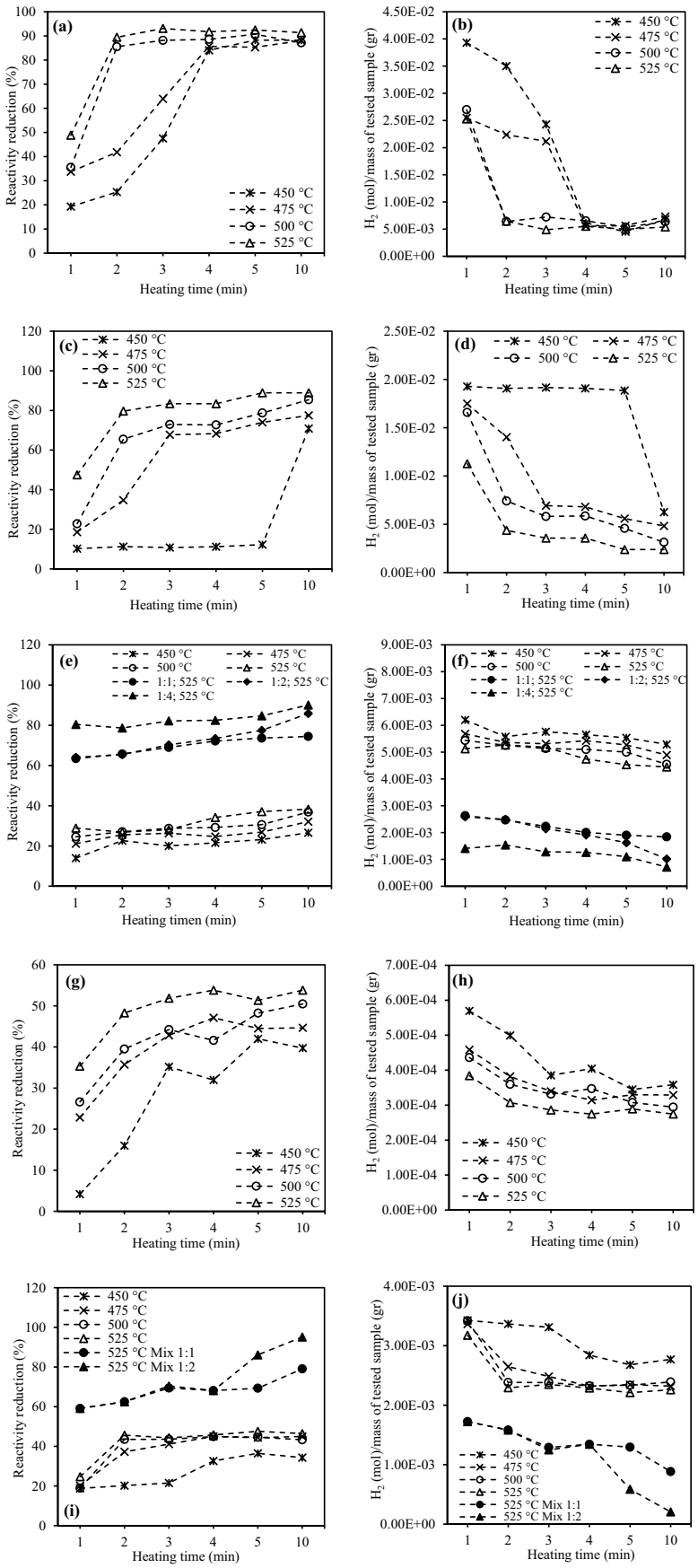

Fig. 5 The reactivity reduction and hydrogen production of pre-treated products vs. heating time at different set temperatures; (**a** and **b**) the S1; (**c** and **d**) the S2; **e** and **f** the S3; **g** and **h** the S4; **i** and **j** the S5

Table 2 Ignition delay time (expressed in seconds) corresponding to the tested samples at different furnace set temperatures

Furnace set point (°C)	Sample									
	S1	S2	S3				S4	S5		
				1:1 (S3: A)	1:2 (S3: A)	1:4 (S3: A)			1:1 (S5: A)	1:2 (S5: A)
450	222	375	–	98	92	85	–	–	125	121
475	178137	217	–	90	85	78	54	–	119	114
500		101	–	84	76	74	43	–	107	101
525	132	64	–	75	70	61	25	–	101	96

by circular economy strategy can be achieved through eco-design, reuse, repair, refurbishment, re-manufacturing and extended producer responsibility (EPR) schemes [64]. Several researchers have studied the aluminothermic reaction in Al/ZnO system leading to the formation of in situ Al_2O_3 at relatively lower temperatures [65–69]. According to Ellingham diagram for oxides (Gaskell 2008), zinc oxide reacts with aluminium as follows [70–72]:

$$2Al + 3ZnO \rightarrow 3Zn + Al_2O_3 \quad (14)$$

According to Eq. (12), this reaction is exothermic. Whilst this reaction is thermodynamically possible at room temperature, the reaction normally occurs at very high temperatures due to kinetics difficulties. A proper combination of suitable alloy addition and thermal process can modify the reaction of the system. For the S3 with addition of 1:1, 1:2 and 1:4 (w:w) ZnO alloy powder, at 525 °C, the ignition delay times are 75, 70 and 61 s, respectively. The results showed that the ignition delay times of the S3 significantly decreased with addition of ZnO alloy powder. Maleki et al. [73] confirmed that a short-time high-temperature contact between aluminium and ZnO leads to the formation of epitaxially grown layers of $ZnAl_2O_4$ and Al_2O_3. The XRD patterns of the oxidation products of the mixed S3 with ZnO alloy powder (with 1:4 w:w) at 525 °C for 5 min are in good agreement with the results of Maleki et al. [73]. Therefore, the addition of ZnO alloy powder can decrease the ignition delay time and, consequently, improve the efficiency of thermal treatment of the S3. This can be certified by the results of reactivity test (Fig. 5), that is, the reaction reactivity of the S3 with addition of ZnO alloy powder is remarkably higher than that of the S3 without additive.

According to the XRD pattern of the S3, at least nine reactions may have taken place between 200 and 1000 °C, which justifies the presence of the nine new oxide compounds identified in the XRD pattern: $CuMn_2O_4$, Sb_2O_4, $ZnAl_2O_4$, $CuAl_2O_4$, Al_2O_3, $MgCr_2O_4$, $ZnAl_2O_4$, ZnO and MoO_2. Regarding the reaction between solid lubricant like Sb_2S_3, Cu and Zn, the Sb_2S_3 oxidation takes place in the temperature range of 300–430 °C, where Sb_2S_3 is converted to Sb_2O_5 and Sb_2O_3 and then to Sb_2O_4 at 570 °C [74, 75]. The study by Martinez and Echeberria [76] was confirmed that the reaction between the metal powders and the lubricant starts at temperatures between 350 and 400 °C, except for the Cu–Sb_2S_3 system, where it starts at a lower temperature (200 °C).

For the S4, observations obtained by ignition test in the tube furnace complete and confirm results obtained by TGA analysis. Both methods prove that oxide film formation is not thermally stabile and if the temperature is below 475 °C, only desorption of organic matters and mineral oil occurs. At 450 °C, the combustion of organic matters proceeds and the presence of CO_2 in off-gas is probable. Although the intermittent flame was observed in this temperature, the S4 could not be ignited, so its ignition delay times are not presented in Table 2. When the S4 is exposed to temperature above 475 °C, the ignition delay times are 54, 43, and 25 s, respectively. As a result of ignition, the degradation of organic parts is complete, and only the inorganic parts remain, which have been tested for their reactivity. The ignition delay time is considerably affected by the heating temperature, especially, when it increased from 500 to 525 °C. The corresponding reactivity values of the combustion products confirmed that for proper decreasing of reactivity, the S4 needs to remain in a furnace for at least 4 min at 525 °C. The reactivity of the S4 in a highly alkaline solution is illustrated in Fig. 5(d). However, reactivity of the S4 with deionised water during a month observation was zero.

In the S5, organic compounds were decomposed after exposure to higher temperature, without occurring ignition. The reactivity test on the remaining mass after exposure to high temperature showed that the thermal treatment of the S5 without additive is not sufficient to reduce the reactivity of this sample. Therefore, the S5 was blended with ZnO alloy powder with specific proportions of 1:1 and 1:2 (w:w). The ignition tests demonstrated that adding ZnO alloy powder improves the ignition and decreases the ignition delay time of the S5.

Handling and storage of the samples after pre-treatment

The concept of inherent safety in the process industries utilises the properties of a material or process to eliminate or reduce their hazard [77]. One of the main principles of

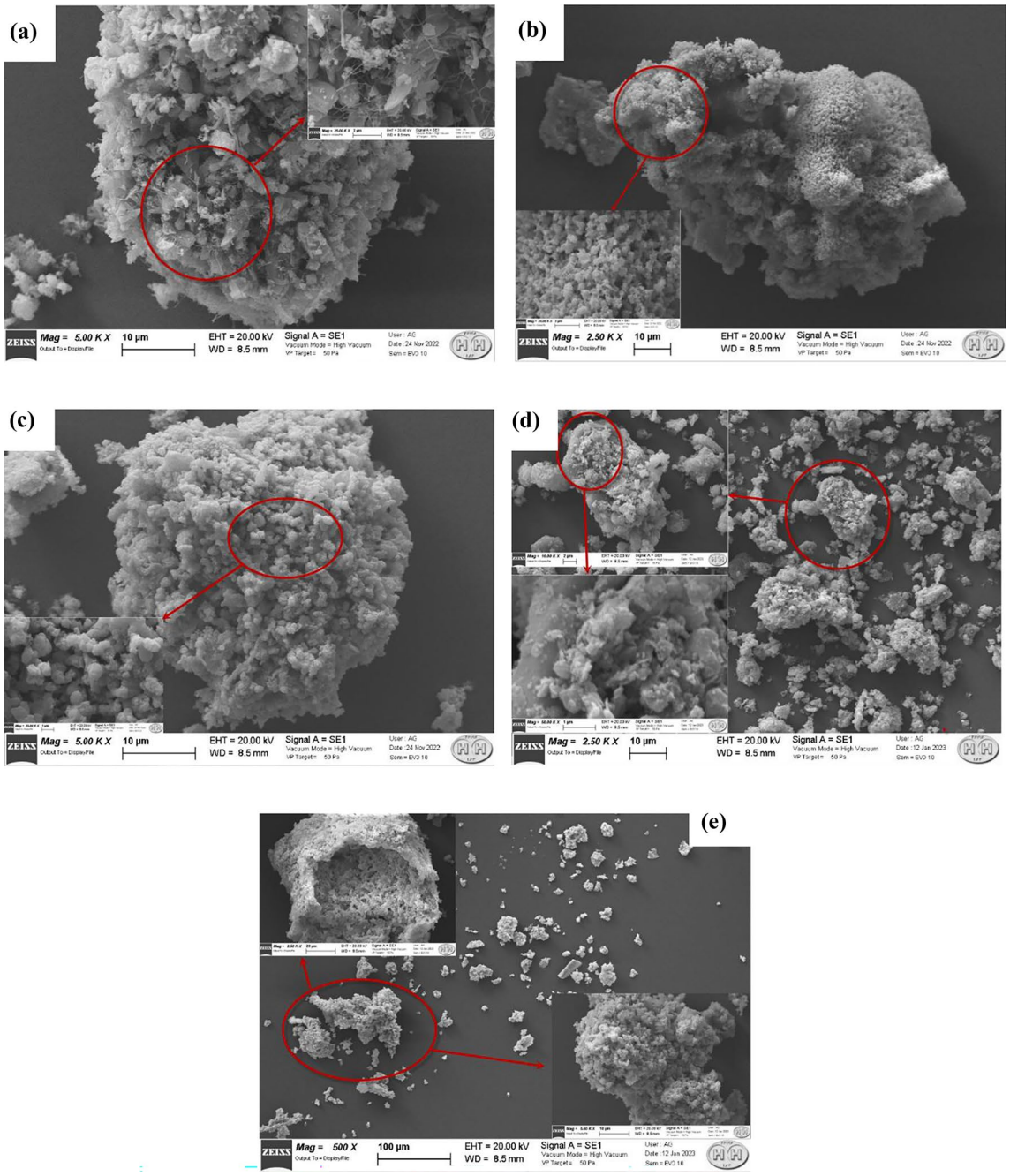

Fig. 6 The SEM images of the pre-treated samples in the furnace; **a** the S1 treated at 475 °C for 4 min; **b** the S2 treated at 475 °C for 4 min; **c** the S3 with additive (1:4) treated at 525 °C for 5 min; **d** the S4 treated at 525 °C for 5 min; **e** the S5 with additive (1:2) treated at 525 °C for 10 min

the inherent safety is to moderate the hazardous materials in their less severe forms. Amyotte and Eckhoff [28] suggested that inertisation of powders or the modification of their composition by the admixture of solid inertants, reducing dust cloud formation by increasing particle size resulting in a decrease in powder reactivity, and preventing hybrid mixtures (which involve the mixture of flammable dust, gas or solvent) can all be helpful in reactive powders modification. According to these suggestions, in this study, a thermal oxidation process was carried out on the aluminium alloy waste powders to modify the composition, morphology and hydrogen gas production capacity of the samples. Although all the raw samples react with DO water, any of the pre-treated samples did not react with DO water even after a month. Nevertheless, consideration must be given to hazard prevention and mitigation when transporting,

storing and landfilling aluminium reactive powders. Great care must be taken to prevent the contact of strong acids (e.g. HCl, H2SO4, HNO_3), oxidising agents (e.g. perchlorates, peroxides, permanganates, chlorates, nitrates, chlorine, bromine and fluorine), acid chlorides, strong bases (e.g. NaOH, KOH), chlorinated hydrocarbons and alcohols.

For raw aluminium powder wastes, attention to the general safety in the working spaces is not enough. It is strongly recommended to avoid any condition that will suspend or float powder particles in the air, creating a dust cloud. It is better if powder is transferred from one container to another using a non-sparking, conductive metal scoop with the most minimal amount of agitation. Moreover, great care must be taken to prevent the contact of water with the non-treated samples. Also, as a result of static electricity discharge, an electric spark can be generated, causing powder particles surrounding the spark to reach temperatures above their ignition temperature, causing a fire or explosion. Therefore, anything that produces a spark, such as an electric switch, a broken light bulb, a commutator on an electric motor, or a loose electric power connection (even a metal-to-metal impact), can cause an explosion of pre-treated aluminium waste powders. An explosion can be caused even by continuous metal-to-metal rubbing (as in a dry sleeve bearing).

Conclusion

Pre-treatment at low–medium temperatures is widely applicable in the context of clean production and sustainable development because of reducing disposal and recycling difficulties. Considering the thermal characteristics of aluminium waste powders, the pre-treatment of grinding filter powder samples was chosen to be carried out under medium-temperature condition. According to the TGA profiles of the samples, the reactive powders were treated at temperatures 450, 475, 500 and 525 °C, using a tubular furnace. Moreover, the ignition delay time of each sample was obtained by post-processing the sequential images of the sample inside the tubular furnace. The results of volume of gas released following the reaction between aluminium waste and NaOH solution showed that the pre-treatment efficiency was strongly dependent on the ignition delay time of the sample at each set temperature. The results show that the medium-temperature pre-treatment can effectively reduce the reactivity of sample when the heating time was higher than the ignition delay time of each sample. The promoting effects of ZnO alloy powder on the ignition and combustion performance of two samples, which could not be ignited at tested temperatures and retention times, were studied. It showed that ZnO alloy powder can dramatically decrease the ignition delay time and initial reaction temperature between aluminium and air inside the furnace.

Supplementary Information The online version contains supplementary material available at https://doi.org/10.1007/s10163-024-01904-y.

Acknowledgements We acknowledge the Brixiambiente Srl for supporting our project financially and preparing the laboratory material and equipment.

Funding Open access funding provided by Università degli Studi di Brescia within the CRUI-CARE Agreement.

Declarations

Conflict of interest The authors declare that they have no known competing financial interests or personal relationships that could have appeared to influence the work reported in this paper.

References

1. Tsakiridis PE, Oustadakis P, Agatzini-Leonardou S (2013) Aluminium recovery during black dross hydrothermal treatment. J Environ Chem Eng 1:23–32. https://doi.org/10.1016/j.jece.2013.03.004
2. Gil A (2005) Management of the salt cake from secondary aluminium fusion processes. Ind Eng Chem Res 44(23):8852–8857. https://doi.org/10.1021/ie050835o
3. Yoshimura HN, Abreu AP, Molisani AL, de Camargo AC, Portela JCS, Narita NE (2008) Evaluation of aluminium dross waste as raw material for refractories. Ceram Int 34:581–591. https://doi.org/10.1016/j.ceramint.2006.12.007
4. EC 2000. Commission Decision 2000/532/EC of 3 May 2000 replacing Decision 94/3/EC establishing a list of wastes pursuant to Article 1(a) of Council Directive 75/442/EEC on waste and Council Decision 94/904/EC establishing a list of hazardous waste pursuant to Article 1(4) of Council Directive 91/689/EEC on hazardous waste. http://data.europa.eu/eli/dec/2000/532/oj
5. Amer AM (2002) Extracting aluminium from dross tailings. J Mater 54(11):72–75. https://doi.org/10.1007/BF02709754
6. Australian Gov. Dept. of the Environment and Water Resources. 2007. Proposal to regulate salt slag under the hazardous waste (Regulation of Exports and Imports) regulations 1996.
7. Lucheva B, Tsonev Ts, Petkov R (2005) Non-waste aluminium dross recycling. J Univ Chem Technol Metall 40(4):335–338
8. Miškufová A, Štifner T, Havlik T, Jančok J (2006) Recovery of valuable substances from aluminium dross. Acta Metall Slovaca 12:303–312
9. Shinzato MC, Hypolito R (2005) Solid waste from aluminium recycling process: Characterization and reuse of its economically valuable constituents. Waste Manage J 25(1):37–46. https://doi.org/10.1016/j.wasman.2004.08.005

10. Calder GV, Stark TD (2010) Aluminium reactions and problems in municipal solid waste landfills. Pract Period Hazard Toxic Radioact Waste Manage 14(4):258–265. https://doi.org/10.1061/(ASCE)HZ.1944-8376.0000045
11. Arm M, Lindeberg J. Gas generation in incinerator ash; 2015. https://www.researchgate.net/publication/266467653.
12. Petrovic J, Thomas G (2011) Reaction of aluminium with water to produce hydrogen US. Dep Energy. https://doi.org/10.2172/1219359
13. Campbell T, Kalia RK, Nakano A, Vashishta P (1999) Dynamics of oxidation of aluminium nanoclusters using variable charge molecular-dynamics simulations on parallel computers. Am Phys Soc 82(24):4866–4869. https://doi.org/10.1103/PhysRevLett.82.4866
14. Emsley J (1991) The elements, 2nd edn. Oxford University Press, UK
15. Trunov MA, Schoenitz M, Dreizin EL (2005) Ignition of aluminium powders under different experimental conditions. Propell Explos Pyrot 30:36–43. https://doi.org/10.1002/prep.200400083
16. Trunov MA, Schoenitz M, Zhu X, Dreizin EL (2005) Effect of polymorphic phase transformations in Al2O3 film on oxidation kinetics of aluminium powders. Combust Flame 140:310–318. https://doi.org/10.1016/j.combustflame.2004.10.010
17. Shmelev V, Nikolaev V, Lee JH, Yim C (2016) Hydrogen production by reaction of aluminium with water. Int J Hydrogen Energy 41:16664e73. https://doi.org/10.1016/j.ijhydene.2016.05.159
18. Rosenband V, Gany A (2010) Application of activated aluminium powder for generation of hydrogen from water. Int J Hydrog Energy 35:10898–10904. https://doi.org/10.1016/j.ijhydene.2010.07.019
19. Nithiya A, Saffarzadeh A, Shimaoka T (2018) Hydrogen gas generation from metal aluminium-water interaction in municipal solid waste incineration (MSWI) bottom ash. Waste Manag 73:342–350. https://doi.org/10.1016/j.wasman.2017.06.030
20. Stark TD, Martin JW, Gerbasi GT, Thalhamer T, Gortner RE (2012) Aluminium waste reaction Indicators in a municipal solid waste landfill. J Geotech Geoenviron 138(3):252–261. https://doi.org/10.1061/(ASCE)GT.1943-5606.0000581
21. Marmo L, Cavallero D, Debernardi ML (2004) Aluminium dust explosion risk analysis in metal workings. J Loss Prev Process Ind 17:449–465. https://doi.org/10.1016/j.jlp.2004.07.004
22. Marmo L, Piccinini N, Danzi E (2015) Small magnitude explosion of aluminium powder in an abatement plant: a telling case. Process Safety Environ Prot 98:221–230. https://doi.org/10.1016/j.psep.2015.06.014
23. Marmo L, Riccio D, Danzi E (2017) Explosibility of metallic waste dusts. Process Saf Environ Prot 107:69–80. https://doi.org/10.1016/j.psep.2017.01.011
24. Cavallero D, Debernardi ML, Marmo L, Piccinini N (2004) Two aluminium powder explosion that occurred in superficial finishing plants. In: Spitzer C, Schmocker U, Dang VN (eds) International conference on probabilistic safety assessment and management PSAM7, Berlin 14–18 June. Springer, London, London, pp 3402–3407
25. Lembo F, Dalla Valle P, Marmo L, Patrucco M, Debernardi ML (2001) Aluminium airborne particles explosions: risk assessment and management at Northern Italian factories. European Safety and Reliability International Conference, Torino, Italy, pp. 16–20
26. Miao N, Zhong S, Yu Q (2016) Ignition characteristics of metal dusts generated during machining operations in the presence of calcium carbonate. J Loss Prev Process Ind 40:174–179. https://doi.org/10.1016/j.jlp.2015.12.022
27. Keown D (2016) Aluminium metal combustible dust explosion from improper design, construction and use of dust collection system sends two employees by life flight to burn centers. J Occup Environ Hyg 13(9):D135–D137. https://doi.org/10.1080/15459624.2016.1177643
28. Amyotte PR, Eckhoff RK (2010) Dust explosion causation, prevention and mitigation: an overview. J Chem Health Saf 17(1):15–28
29. Kumar A, Madden DG, Lusi M, Chen K, Daniels EA, Curtin T, Perry JJ, Zaworotko MJ (2015) Direct air capture of CO2 by physisorbent materials. Angew Chem Int Ed 54:14372–14377. https://doi.org/10.1002/anie.201506952
30. Sodhi GS, Kaur J (2001) Powder method for detecting latent fingerprints: a review. Forensic Sci Int. https://doi.org/10.1016/s0379-0738(00)00465-5
31. Karlsson PM, Baeza A, Palmqvist AEC, Holmberg K (2008) Surfactant inhibition of aluminium pigments for waterborne printing inks. Corros Sci 50:2282–2287. https://doi.org/10.1016/j.corsci.2008.06.014
32. Sverak TS, Baker CGJ, Kozdas O (2013) Efficiency of grinding stabilizers in cement clinker processing. Miner Eng 43–44:52–57. https://doi.org/10.1016/j.mineng.2012.08.012
33. Nie H, Schoenitz M, Dreizin EL (2012) Calorimetric investigation of the aluminium–water reaction. Int J Hydrogen Energy 37:11035–11045. https://doi.org/10.1016/j.ijhydene.2012.05.012
34. Shimamura K, Shimojo F, Kalia RK, Nakano A, Nomura K, Vashishta P (2014) Hydrogen-on-demand using metallic alloy nanoparticles in water. Nano Lett 14:4090–4096. https://doi.org/10.1021/nl501612v
35. Pathak C, Dodkar P (2020) Effect of shot blasting and shot peening parameters on residual stresses induced in connecting rod. Trans Indian Inst Met 73(3):571–576. https://doi.org/10.1007/s12666-020-01866-3
36. Hou N, Wang M, Wang B, Zheng Y, Zhou S, Song C (2022) Fundamental functions of physical and chemical principles in the polishing of titanium alloys: mechanisms and problems. Int J Adv Manuf Technol 118:2079–2097. https://doi.org/10.1007/s00170-021-08100-4
37. EC 2014. Commission Decision 2014/955/EU of 18 December 2014 amending Decision 2000/532/EC on the list of waste pursuant to Directive 2008/98/EC of the European Parliament and of the Council. http://eurlex.europa.eu/legalcontent/EN/TXT/PDF/?uri=CELEX:32014D0955&rid=1
38. EC 2014. Commission Regulation (EU) No 1357/2014 of 18 December 2014 replacing Annex III to Directive 2008/98/EC of the European Parliament and of the Council on waste and repealing certain Directives. Official Journal of the European Union. 19.12.2014. L 365/89.
39. Alviani VN, Setiani P, Uno M, Oba M, Hirano N, Watanabe N (2019) Mechanisms and possible applications of the Al-H2O reaction under extreme pH and low hydrothermal temperatures. Int J Hydrogen Energy 44:29903–29921. https://doi.org/10.1016/j.ijhydene.2019.09.152
40. Zhu B, Li F, Sun Y, Wu Y, Shi W, Han W, Qichang W, Qi W (2019) Enhancing ignition and combustion characteristics of micron-sized aluminium powder in steam by adding sodium fluoride. Combust Flame 205:68–79. https://doi.org/10.1016/j.combustflame.2019.02.007
41. Shi W, Sun Y, Zhu B, Liu J (2021) Sodium fluoroaluminate promoting the combustion of micron-sized aluminium powder with different particle sizes in carbon dioxide. Energy 226:120393
42. Cai J, Liang Y, Jia R, Amyotte P, Chen Y, Yuan C (2022) Investigating the explosion hazard of hydrogen produced by activated aluminium in a modified Hartmann tube. Int J Hydrogen Energy 47:15933–15941. https://doi.org/10.1016/j.ijhydene.2022.03.070
43. Xiao F, Li J, Zhou X, Yang R (2018) Preparation of mechanically activated aluminium rich Al-Co_3O_4 powders and their thermal properties and reactivity with water steam at high temperature.

Combust Sci Technol 190:1–15. https://doi.org/10.1080/00102202.2018.1477771
44. Zhou X, Zou M, Huang F, Yang R, Guo X (2017) Effect of organic fluoride on combustion agglomerates of aluminized HTPB solid propellant. Propellants, Explos Pyrotech 42:417–422. https://doi.org/10.1002/prep.201600096
45. Esposito PH, Leroux C, Heresanu V, Neisius T, Madigou V, Denoyel R, Coulet MV (2020) Influence of texture and microstructure on the reactivity of aluminum powders. Materialia 14:100880
46. Chen L, Song WL, Lv J, Wang L, Xie CS (2009) Effect of heating rates on TG-DTA results of aluminium nanopowders prepared by laser heating evaporation. J Therm Anal Calorim 96:141–145. https://doi.org/10.1007/s10973-008-9374-7
47. Kwon YS, Moon JS, Ilyin AP, Gromov AA, Popenko EM (2004) Estimation of the reactivity of aluminium superfine powders for energetic applications. Combust Sci Technol 176:277–288. https://doi.org/10.1080/00102200490255992
48. Ilin AP, Gromov AA, Yablunovskii GV (2001) Reactivity of aluminium powders. Combust Explos Shock Waves 37(4):418–422. https://doi.org/10.1023/A:1017997911181
49. Rufino B, Boulc'h, F., Coulet, M.-V., Lacroix, G., Denoyel, R. (2007) Influence of particles size on thermal properties of aluminium powder. Acta Mater 55:2815–2827. https://doi.org/10.1016/j.actamat.2006.12.017
50. Li R, Fang Y, Yang T, Sun Y, Li Y (2011) Influence factor of hydrogen generation from aluminium-water reaction. IEEE. https://doi.org/10.1109/CDCIEM.2011.58
51. Mondolfo LF (1976) Aluminium Alloys: Structure and Properties. Butterworths and Co., Ltd., London, 806. https://doi.org/10.1016/B978-0-408-70932-3.50404-6
52. Saravanan RA, Molina JM, Narciso J, Garcia-Cordovilla C, Louis E (2001) Effects of nitrogen on the surface tension of pure aluminium at high temperatures. Scr Mater 44(6):965–997. https://doi.org/10.1016/S1359-6462(00)00688-6
53. Yagodnikov DA, Andreev EA, Vorobev VS, Glotov OG (2006) Ignition, combustion, and agglomeration of encapsulated aluminium particles in a composite solid propellant. I. theoretical study of the ignition and combustion of aluminium with fluorine-containing coatings. Combust Explos Shock Waves 42:534–542. https://doi.org/10.1007/s10573-006-0085-8
54. Ilin AP, Yablunovskii GV, Gromov AA, Popenko EM, Bychin NV (1999) Combustion of mixtures of ultrafine powders of aluminium and boron in air. Combust Explos Shock Waves 35:656–659. https://doi.org/10.1007/BF02674539
55. Parr, T.P., Johnson, C., Hanson-Parr, D., Higa, K., Wilson, K. 2003. Evaluation of advanced fuels for underwater propulsion. In: 39th JANNAF combustion subcommittee meeting. NASA Technical Reports Serve.
56. Ohkura Y, Rao PM, Zheng XL (2011) Flash ignition of al nanoparticles: mechanism and applications. Combust Flame 158:2544–2548. https://doi.org/10.1016/j.combustflame.2011.05.012
57. Rozenband VI, Afanaseva LF, Lebedeva VA, Chernenko EV (1990) Activation of ignition of aluminium and its mixtures with oxides by chromium chloride. Combust Explos Shock Waves 26:13–15
58. Shi W, Dai B, Zhu B, Sun Y, Chen Y (2019) Potassium fluoride improving the ignition and combustion performance of micron-sized aluminium particles in high temperature water vapor. energy sources a: recovery util. Environ Eff 1556–7036:1556–7230. https://doi.org/10.1080/15567036.2019.1670289
59. Rosenband V, Gany A (2007) Agglomeration and ignition of aluminium particles coated by nickel. Int J Energ Mater Chem Prop 6:141–149. https://doi.org/10.1615/IntJEnergeticMaterialsChemProp.v6.i2.10
60. Shoshin YL, Mudryy RS, Dreizin EL (2002) Preparation and characterization of energetic Al-Mg mechanical alloy powders. Combust Flame 128(3):259–269. https://doi.org/10.1016/S0010-2180(01)00351-0
61. Parimi VS, Huang SD, Zheng XL (2017) Enhancing ignition and combustion of micron-sized aluminium by adding porous silicon. Proc Combust Inst 36:2317–2324. https://doi.org/10.1016/j.proci.2016.06.185
62. Zhu B, Wang J, Wang Q, Sun Y, Chen W, Wang J (2022) Promotional effect of silica on the combustion of nano-sized aluminium powder in carbon dioxide. Chin J Aeronaut 35(4):245–252. https://doi.org/10.1016/j.cja.2021.05.020
63. Tsao LC, Chiang MJ, Lin WH, Cheng MD, Chung TH (2002) Effects of zinc additions on the microstructure and melting temperatures of Al-Si-Cu filler metals. Mater Charact 48:341–346. https://doi.org/10.1016/S1044-5803(02)00276-0
64. Busu, M. 2019. Adopting Circular economy at the European Union level and its impact on economic growth. Soc. Sci. 2019, 8(5), 159. https://doi.org/10.3390/socsci8050159
65. Maleki A, Panjepour M, Niroumand B, Meratian M (2010) Mechanism of zinc oxide aluminium aluminothermic reaction. J Mater Sci 45:5574–5580. https://doi.org/10.1007/s10853-010-4619-9
66. Durai TG, Das K, Das S (2007) Wear behavior of nano structured Al(Zn)/Al2O3 and Al(Zn)–4Cu/Al2O3 composite materials synthesized by mechanical and thermal process. Mater Sci Eng A 471:88–94. https://doi.org/10.1016/j.msea.2007.05.060
67. Durai TG, Das K, Das S (2008) Al(Zn)–4Cu/Al2O3 in-situ metal matrix composite synthesized by displacement reactions. J Alloy Compd 457:435–439. https://doi.org/10.1016/j.jallcom.2007.02.142
68. Durai G, Das K, Das S (2008) Corrosion behavior of Al–Zn/Al2O3 and Al–Zn–X/Al2O3 (X = Cu, Mn) composites synthesized by mechanical–thermal treatment. J Alloy Compd 462:410–415. https://doi.org/10.1016/j.jallcom.2007.08.073
69. Hedayati A, Golestan Z, Ranjbar Kh, Borhani GH (2011) Effect of ball milling on formation of ZnAl2O4 by reduction reaction of ZnO and Al powder mixture, Powder Metall. Met Ceram 50:268–274. https://doi.org/10.1007/s11106-011-9328-7
70. Karimzadeh F, Enayati MH, Tavoosi M (2008) Synthesis and characterization of Zn/Al2O3 nanocomposite by mechanical alloying. Mater Sci Eng A 486:45–48. https://doi.org/10.1016/j.msea.2007.08.059
71. Durai TG, Das K, Das S (2007) Synthesis and characterization of Al matrix composites reinforced by in situ alumina particulates. Mater Sci Eng A 445–446:100–105. https://doi.org/10.1016/j.msea.2006.09.018
72. Tavoosi M, Karimzadeh F, Enayati MH (2008) Fabrication of Al–Zn/α-Al2O3 nanocomposite by mechanical alloying. Mater Lett 62:282–285. https://doi.org/10.1016/j.matlet.2007.05.017
73. Maleki A, Hosseini N, Niroumand B (2018) A review on aluminothermic reaction of Al/ZnO system. Ceram Int 44(1):10–23
74. Lee WK, Rhee TH, Kim HS, Jang H (2013) Effects of Antimony Trisulfide (Sb2S3) on sliding friction of automotive brake friction materials. Met Mater Int 19:1101. https://doi.org/10.1007/s12540-013-5027-x
75. Cho MH, Ju J, Kim SJ, Jang H (2006) Tribological properties of solid lubricants (Graphite, Sb_2S_3, MoS_2) for automotive brake friction materials. Wear 260:855. https://doi.org/10.1016/j.wear.2005.04.003
76. Martinez AM, Echeberria J (2016) Towards a better understanding of the reaction between metal powders and the solid lubricant Sb_2S_3 in a low-metallic brake pad at high temperature. Wear 348–349:27–42. https://doi.org/10.1016/j.wear.2015.11.014
77. Amyotte PR, Pegg MJ, Khan FI (2009) Application of inherent safety principles to dust explosion prevention and mitigation.

Process Saf Environ Protect 87(1):35–39. https://doi.org/10.1016/j.psep.2008.06.007